Properties of foreshocks and aftershocks of the nonconservative self-organized critical Olami-Feder-Christensen model

Agnès Helmstetter*

Institute of Geophysics and Planetary Physics, University of California, Los Angeles, California 90095-1567, USA

Stefan Hergarten

Geodynamics-Physics of the Lithosphere, University of Bonn, Bonn, Germany

Didier Sornette

Department of Earth and Space Sciences and Institute of Geophysics and Planetary Physics, University of California, Los Angeles, California 90095-1567, USA
and Laboratoire de Physique de la Matière Condensée, CNRS UMR 6622, Université de Nice-Sophia Antipolis, Parc Valrose, 06108 Nice, France

Following Hergarten and Neugebauer [Phys. Rev. Lett. **88**, 238501, 2002] who discovered aftershocks and foreshocks in the Olami-Feder-Christensen (OFC) discrete block-spring earthquake model, we investigate to what degree the simple toppling mechanism of this model is sufficient to account for the clustering of real seismicity in time and space. We find that synthetic catalogs generated by the OFC model share many properties of real seismicity at a qualitative level: Omori's law (aftershocks) and inverse Omori's law (foreshocks), increase of the number of aftershocks and of the aftershock zone size with the mainshock magnitude. There are, however, significant quantitative differences. The number of aftershocks per mainshock in the OFC model is smaller than in real seismicity, especially for large mainshocks. We find that foreshocks in the OFC catalogs can be in large part described by a simple model of triggered seismicity, such as the epidemic-type aftershock sequence (ETAS) model. But the properties of foreshocks in the OFC model depend on the mainshock magnitude, in qualitative agreement with the critical earthquake model and in disagreement with real seismicity and with the ETAS model.

I. INTRODUCTION

Describing and modeling the space-time organization of seismicity and understanding the underlying physical mechanisms remain important open challenges. Inspired by statistical regularities such as the Gutenberg-Richter [1] and the Omori's [2] laws, a wealth of mechanisms and models have been proposed. New classes of models inspired or derived from statistical physics accompanied and followed the proposition, repeated several times under various forms in the last 25 years, that the space-time organization of seismicity is similar to the behavior of systems made of elements interacting at many scales that exhibit collective behavior such as in critical phase transitions. This led to the concepts of the critical earthquake, of self-organized criticality, and more generally of the seismogenic crust as a self-organized complex system requiring a so-called system approach.

Our purpose here is to study in depth maybe the simplest model of the class of self-organized critical models that exhibit a phenomenology resembling real seismicity, the so-called Olami-Feder-Christensen (OFC) sandpile model. Large shallow earthquakes are always followed by a very large seismicity rate (called "aftershocks") and are sometimes preceded by an increase of seismicity rate ("foreshocks"). Many different mechanisms have been proposed to explain the occurrence of foreshocks and aftershocks. The OFC model uses only one simple local interaction between discrete fault elements but nevertheless exhibits foreshocks and aftershocks [3]. The motivation of our present work is to study the main characteristics of foreshocks and aftershocks in the OFC model and to understand the mechanisms responsible for earthquake clustering in the OFC model. For this, we will interpret our analysis of the OFC catalogs in the light of two end-member models representing two opposite views of seismicity. The first one, mentioned above, is the critical earthquake model, which views a mainshock as the special outcome of a global self-organized buildup occurring at smaller scales. The second end-member model is called the epidemic-type aftershock sequence (ETAS) model [4], which is a phenomenological construction based on the well-documented Gutenberg-Richter law, the Omori's law, and the scaling of the number of aftershocks with the mainshock size.

The plan of our paper is the following. Section II presents the OFC model, Sec. III summarizes the phenomenology of real seismicity, and Sec. IV presents the critical earthquake model and the ETAS model. Section V presents the results obtained for the OFC model, which are compared with real seismicity and with the two reference models (ETAS and critical earthquake). We discuss in Sec. VI possible mecha-

---

*Present address: Lamont-Doherty Earth Observatory of Columbia University, 61 Route 9W, Palisades, NY 10964, USA.

nisms for foreshocks and aftershocks in the OFC model. Section VII concludes.

II. OLAMI-FEDER-CHRISTENSEN MODEL

The Olami-Feder-Christensen model [5] is defined on a discrete system of blocks or of fault elements on a square lattice, each carrying a force. The force F_i of a given element i that exceeds a fixed threshold F_c (taken equal to 1 without loss of generality) relaxes to zero. Such a toppling increments the forces on its nearest neighbors by a pulse which is α ($\alpha \leqslant 1/4$) times the force F_i of the unstable element:

$$F_i \geqslant F_c \Rightarrow \begin{cases} F_i \rightarrow 0, \\ F_{nn} \rightarrow F_{nn} + \alpha F_i. \end{cases} \tag{1}$$

This loading to nearest neighbors can in turn destabilize these sites, creating an avalanche. Between events, all F_i's increase at the same constant rate, mimicking a uniform tectonic loading. We choose the time scale in such a way that the rate of driving is unity. Then one time unit corresponds to the time needed to reload a site from zero force to its threshold of instability. The OFC model can be obtained as a sandpile analogue of block-spring models [6], with the interpretation

$$\alpha = \frac{1}{n_i + k}, \tag{2}$$

where n_i is the actual number of neighbors of site i. Here n_i is always 4 in the case of a square lattice with rigid-frame boundaries. For free boundary conditions used in this study $n_i = 4$ in the bulk, $n_i = 3$ at the boundaries, and $n_i = 2$ at the corners. The symbol k denotes the elastic constant of the upper leaf springs, measured relatively to that of the other springs between blocks. The OFC model is conservative for $k = 0$ for which $\alpha = 0.25$ and is nonconservative for $k > 0$ for which $\alpha < 0.25$. In the following, we will compare results obtained for $k = 0.5$, 1, 2, and 4—that is, for $\alpha = 0.222$, 0.2, 0.167, and 0.125.

With open or rigid boundary conditions, this model seems to show self-organized criticality (SOC) [7–9] even in the nonconservative case $\alpha < 0.25$. SOC is the spontaneous convergence of the dynamics to a statistically stationary state characterized by a time-independent power law distribution of avalanches. The size of an avalanche is taken to be the spanned area s. The underlying mechanism for SOC seems to be the invasion of the interior by a region spreading from the boundaries, self-organized by the synchronization or phase-locking forces between the individual elements [10].

Long-term correlation between large events have been documented but, only very recently, Ref. [3] found the occurrence of genuine sequences of foreshocks and aftershocks that bear similarities with real earthquake catalogs. This discovery suggests that a unique mechanism is sufficient to produce a Gutenberg-Richter-like distribution as well as realistically looking foreshocks and aftershocks, without the need for viscous crust relaxation or other mechanisms. Similarly, Ref. [11] found critical precursory activity and aftershock sequences in a sandpile model. However, the precursors and

aftershocks resulted from the interplay between the built-in hierarchy of domains and a conservative sandpile dynamics. The remarkable observation of Ref. [3] is that such a hierarchy is not needed for foreshocks and aftershocks to occur, when the sandpile dynamics is dissipative. However, a hierarchy of faults may be needed to obtain a larger number of triggered events than found for the OFC model, in order to be more compatible with real seismicity. Our goal here is to investigate in details the properties of the foreshocks and aftershocks in the simplest situation—i.e., in the OFC model.

Our simulations presented below are performed in two-dimensional square lattices $L \times L$ with $L = 512$, 1024, and 2048. Let us give a correspondence between time and space units in the OFC model and in the real seismicity. If we consider that the lattice of $L = 2048$ blocks represents a fault of 200×200 km (we neglect the asymmetrical aspect ratio of real faults), the minimum earthquake of size $s = 1$ generated by the OFC model has a length of ≈ 0.1 km, corresponding to a magnitude-2 earthquake. The recurrence time of $M \geqslant 5$ earthquakes in Southern California is about 100 days, corresponding to about 1000 days for a region of 200 $\times 200$ km. In the OFC model with $L = 2048$, the recurrence time of an event of size $s > 1000$, equivalent to a magnitude-5 earthquake, is about 1.7×10^{-3}. This gives the correspondence between time units time$_{\text{OFC}}$ in the OFC model and in real seismicity:

$$\text{time}_{\text{OFC}} = 10^{-4} \Leftrightarrow \text{time}_{\text{real}} = 60 \text{ days}. \tag{3}$$

III. PHENOMENOLOGY OF REAL SEISMICITY

The empirical properties of real seismicity discussed in this paper are the following.

(i) *The Gutenberg-Richter (GR) law* [1] states that the density distribution function $P(m)$ of earthquake magnitudes m is

$$P_0(m)dm = b \ln(10) 10^{-b(m-m_d)} dm, \tag{4}$$

with a b value usually close to 1. Here m_d is a lower bound magnitude of detection, such that $P_0(m)$ is normalized to 1 by summing over all magnitudes above m_d.

The qualifying property of SOC in the OFC model is the existence of a GR-like distribution of avalanches sizes. There are several measures of sizes. If we take the size defined as the area s spanned by an avalanche, the distribution of event sizes is given by Eq. (4), where the magnitude m is defined by

$$m = 2 + \log_{10}(s), \tag{5}$$

in analogy with real seismicity. The number of topplings is not exactly equal to s since a site can topple more than once in a given avalanche, possibly being reloaded during its development. However, the difference is negligible for our purpose. No multiple relaxations were observed for $k \geqslant 2$. For $k = 1$, less than 1 multiple relaxation per 100 000 earthquakes was found.

(ii) *The (modified) Omori's law* [2,12,13] describes the decay of the seismicity rate triggered by a mainshock with the time t since the time t_c of the mainshock

$$N_a(t) = \frac{K_a}{(t - t_c + c)^{p_a}}, \qquad (6)$$

with an Omori's exponent p_a close to 1. This decay law can be detected over time scales spanning from weeks up to decades, depending on the mainshock magnitude. The time shift constant c ensures a finite seismicity rate just after the mainshock and is often of the order of minutes.

(iii) *The inverse Omori's law* [12,14,15] describes the average increase of seismicity observed before a mainshock and is like Eq. (6) with $t - t_c$ replaced by $t_c - t$:

$$N_f(t) = \frac{K_f}{(t_c - t + c)^{p_f}}, \qquad (7)$$

with the inverse Omori's exponent p_f usually close to or slightly smaller than p_a [16]. In contrast with Omori's law which can be clearly observed for a single mainshock, the inverse Omori's law (7) can only be found by averaging the seismicity rate before a large number of mainshocks [23], because there are huge fluctuations of the rate of seismicity before individual mainshocks [23].

(iv) *The number of aftershocks increases* with the magnitude m of the mainshock as

$$N_a(m) \sim 10^{\alpha_a m}, \qquad (8)$$

where the exponent α_a is usually found in the range 0.5–1 (see [17] and references therein). This value of the exponent α_a may reveal a fractal spatial distribution of aftershocks [17].

(v) *Aftershock diffusion*. Several studies have reported "aftershock diffusion," the phenomenon of expansion or migration of aftershock zone with time [18,19]. However, the present state of knowledge on aftershock diffusion is confusing because contradictory results have been obtained, some showing almost systematic diffusion whatever the tectonic setting and in many areas in the world, while others do not find evidence of aftershock diffusion [20,21]. The shift in time from the dominance of the aftershock activity clustered around the mainshock at short times after the mainshock to the delocalized background activity at large times may give rise to an apparent diffusion of the seismicity [21].

(vi) *Foreshock migration*. Foreshock migration towards the mainshock as time increases up to the time of the mainshock has also been documented [12,22,23] but may be due to an artifact of the background activity, which dominates the catalog at long times and distances from the mainshock [23]. Indeed, by an argument symmetrical to that for aftershocks, the shift in time from the dominance of the background activity at large times before the mainshock to that of the foreshock activity clustered around the mainshock at times just before it may be taken as an apparent inverse diffusion of the seismicity rate.

(vii) *The average distance R_a between aftershocks and the mainshock rupture epicenter* has been found to be proportional to the rupture size of the mainshock, leading to the scaling law [24]

$$R_a \sim 10^{0.5m} \sim s^{0.5}, \qquad (9)$$

relating R_a and the mainshock magnitude m or the mainshock rupture surface s. A similar law is suggested to hold for the average distance R_f between foreshocks and the mainshock [25,26], but other studies [23] did not observe an increase of R_f with m.

(viii) *Foreshock magnitude distribution*. Many studies have found that the apparent b value of the magnitude distribution of foreshocks is smaller than that of the magnitude distribution of the background seismicity and of aftershocks (see [16] and references therein).

(ix) *Number of foreshocks and aftershocks per mainshock.* Foreshocks are less frequent than aftershocks [12,15,27]. The ratio of foreshock to aftershock numbers is in the range 2–4 for $m = 5 - 7$ mainshocks, when selecting foreshocks and aftershocks at a distance in the range $R = 50 - 500$ km from the mainshock and for a time in the range $T = 10 - 100$ days before or after the mainshock [12,15,20,22,27].

IV. END-MEMBER MODELS OF SEISMICITY: ETAS AND CRITICAL EARTHQUAKE MODELS

A. ETAS model

The epidemic-type aftershock sequence model was introduced in [4] and in [28] (in a slightly different form). Contrary to what its name may imply, it is not only a model of aftershocks but a general model of seismicity. This model avoids the division between foreshocks, mainshocks, and aftershocks because it uses the same laws to describe all earthquakes. Because of its simplicity, it is natural to consider it as a null hypothesis to explain the OFC catalogs and real data. Its choice as a reference is also natural because it is nothing but a branching model of earthquake interactions and can thus be considered as a mean-field approximation of more complex interaction processes. Branching processes can also be considered as natural mean-field approximations of SOC models and in particular of the OFC model [29] (see also Chap. 15 in [9]). The approximation consists usually in the fact that branching models neglect the loops occurring in the cascade characterizing a given avalanche. Note that standard branching models study the development of a single avalanche while the ETAS model describes a catalog of earthquakes.

The ETAS model uses three of the above empirical laws as direct inputs [Gutenberg-Richter law (4), Omori's law (6), and aftershock scaling law (8)]. In the ETAS model, each event of magnitude m triggers its own primary aftershocks (considered as point processes) according to the following distribution in time and space:

$$\phi_m(r,t) dr dt = K 10^{\alpha_a m} \frac{\theta c^\theta dt}{(t + c)^{1+\theta}} \frac{\mu d^\mu dr}{(r + d)^{1+\mu}}, \qquad (10)$$

where r is the spatial distance to the main event. The spatial regularization distance d accounts for the finite rupture size. The power law kernel in space with exponent μ quantifies the fact that the distribution of distances between pairs of events is well described by a power law [30]. The ETAS model assumes that each primary aftershock may trigger its

own aftershocks (secondary events) according to the same law, the secondary aftershocks themselves may trigger tertiary aftershocks, and so on, creating a cascade process. The exponent $1 + \theta$ is not the observable Omori's exponent p_a but defines the "bare" Omori's law for the aftershocks of first generation. The whole series of aftershocks, integrated over the whole space, can be shown to lead to a "renormalized" (or dressed) Omori's law, which is the total observable Omori's law [31]. To prevent the process from dying out, a small Poisson rate of uncorrelated seismicity driven by plate tectonics is added to represent the effect of the tectonic loading in earthquake nucleation.

The ETAS model predicts the following properties.

(i) The total number of triggered events (including all generations of aftershocks) has the same average power law increase (8) with the mainshock size s as the number of first-generation aftershocks [31].

(ii) The ETAS model predicts a renormalized Omori's law (for aftershocks of all generations) different from the "bare" Omori's law $\sim 1/(t+c)^{1+\theta}$ defined in Eq. (10) for the first-generation aftershocks, with a renormalized exponent $p_a \leq 1 + \theta$ [31].

(iii) An inverse Omori's law for foreshocks is found to result simply from the existence of the "bare" Omori's law (10) for aftershocks and from cascades of multiple triggering [16].

(iv) The ETAS model predicts a modification of the magnitude distribution (4) before a mainshock of magnitude m_M, characterized by an increase of the proportion of large earthquakes according to the following expression [16]:

$$P(m|m_M) = [1 - Q(t)]P_0(m) + Q(t)dP(m), \quad (11)$$

where $P_0(m)$ is the unconditional GR distribution (4),

$$dP(m) = b' \ln(10) 10^{-b'(m-m_0)}, \text{ with } b' = b - \alpha_a, \quad (12)$$

and

$$Q(t) = \frac{C}{(t_c - t)^\nu}, \text{ with } \nu = \frac{\theta(b - \alpha_a)}{\alpha_a}, \quad (13)$$

t_c is the time of the mainshock, and C is a numerical constant. The prediction (11) with Eqs. (12) and (13) is that the magnitude distribution is modified upon the approach of a mainshock by developing a bump in its tail which takes the form of a growing additive power-law contribution with a new b' value.

(v) In the ETAS model, the properties of foreshocks are independent of the mainshock magnitude, because the magnitude of each event is not predictable but is given by the GR law with a constant b value [16].

(vi) By the mechanism of cascades of triggering, the ETAS model also predicts the possibility for large distance and long-time buildup of foreshock activity as well as the migration of foreshocks toward mainshocks [21,23].

These predictions of the ETAS model are in good agreement with observations of the seismicity in Southern California [23].

B. Critical earthquake model

Maybe the first work on accelerated seismicity leading to the concept of criticality is [25], who observed that the trailing total sum of the source areas of medium-size earthquakes accelerates with time on the approach to a large earthquake. The theoretical ancestor of the critical earthquake concept can probably be traced back to [32], who used a branching model to illustrate a cascade of earthquake ruptures culminating in complete collapse interpreted as a great one. Reference [33] proposed a renormalization group analysis of a percolation model of damage and rupture prior to an earthquake paralleling [34], which emphasized the critical point nature of earthquake rupture following an inverse cascade from small to large scales. References [35,36] were probably the first ones to introduce the idea of a time-to-failure analysis in the form of a second-order nonlinear differential equation, which for certain values of the parameters leads to a solution of the form of a time-to-failure equation describing the power-law acceleration of an observable with time:

$$\epsilon(t) \propto A - B(t_c - t)^z, \quad (14)$$

where $\epsilon(t)$ is, for instance, the cumulative Benioff strain (square root of earthquake energy), A and B are positive constants, t_c is the critical time of the mainshock, and $0 < z < 1$ is a critical exponent. Reference [37] introduced Eq. (14) to fit and predict large earthquakes. Their justification of Eq. (14) was a mechanical model of material damage. Reference [37] did not mention the critical earthquake concept. Reference [38] proposed to reinterpret [37] and all these previous works and to generalize them using a statistical physics framework. The concept of a critical earthquake described in Ref. [38] corresponds to viewing a major or great earthquake as a genuine critical point in the statistical physics sense. In a nutshell, a critical point is characterized by long-range correlations and by power laws describing the behavior of various observables on the approach to the critical point. This concept has been elaborated in subsequent works [11,26,39–46]. The critical earthquake model predicts a power-law increase of the number and of the average energy of foreshocks before large earthquakes. According to this model, the modification of seismic activity should be more apparent before larger mainshocks. Therefore, we should measure a positive value for α_f characterizing foreshocks. The critical model also predicts that the preparation zone or foreshocks cluster size R_f should increase with the mainshock size s as $R_f \sim s^{q_f}$ with $q_f > 0$, as observed by [25,26] (see [40] for an extended compilation and discussion).

V. PROPERTIES OF THE SYNTHETIC SEISMICITY GENERATED BY THE OFC MODEL

A. Definitions of foreshocks and aftershocks

Extending the discovery of [3], we found that all the properties of real seismicity discussed in Sec. III exist at least at a qualitative level in synthetic catalogs generated by the OFC model. Earthquakes in the OFC model are clustered in space and time. The seismicity rate after a large event ("main-

shock") is much larger than on average, due to the existence of "aftershocks," triggered by the mainshock. The seismicity rate before a mainshock is also larger than the average rate: events occurring at short times and short distances before a mainshock are usually defined as "foreshocks." The definition of "mainshocks," "foreshocks," and "aftershocks" is always arbitrary, and several methods have been proposed [21,47]. We thus consider several alternative definitions.

Definition d=0. We adopt the usual definition and define as a "mainshock" any earthquake of magnitude m which was not preceded or followed by a larger earthquake in a time window of length $T(m)$ equal to 1% of the average return time of an earthquake of magnitude m. Foreshocks (aftershocks) are then selected as all earthquakes occurring within the time $T(m)$ before (after) a mainshock. By definition, aftershocks and foreshocks for $d=0$ are thus smaller than their mainshock. The value of $T(m)$ is chosen such that the seismicity rate in the time interval $[-T(m);T(m)]$ before and after a mainshock of magnitude m is much larger than the average ("background") rate. Recent empirical and theoretical studies suggest that this definition might be arbitrary and physically artificial [17,20,23,28,48–50]. Indeed, the magnitude of an earthquake in real seismicity seems to be unpredictable [17]; therefore, the same mechanisms responsible for the triggering of small earthquakes (usual "aftershocks" for $d=0$) may also explain the triggering of larger earthquakes (defined as "mainshocks" for $d=0$) [23]. We thus use two other definitions of foreshocks and aftershocks, which do not constrain aftershocks and foreshocks to be smaller than the mainshock, in order to test how the selection procedure impacts on foreshock and aftershock properties.

Definition d=1. A mainshock is now defined as any earthquake of magnitude m that was not preceded by a larger earthquake within the time window $T(m)$, but can be followed by a larger event. This rule aims to select as aftershocks the events that have been triggered directly or indirectly by the mainshock, removing the influence of large earthquakes that occurred before the mainshock. Foreshocks are thus smaller than mainshocks but aftershocks can be larger.

Definition d=2. Same as $d=1$ without any constraint on the magnitude of foreshocks, aftershocks and mainshocks. Each event is considered as a mainshock. For foreshocks, this corresponds to the "type-II" foreshocks introduced in [16,23] in order to remove any spurious dependence of foreshock properties on the mainshock magnitude.

We use these three definitions in order to understand the origin of foreshocks and aftershocks in the OFC model: are foreshocks witnesses of a "critical" acceleration of seismicity before the mainshock or is a mainshock triggered by the foreshocks, the same way as aftershocks are triggered by the mainshock? Can we explain the triggering of a large earthquake by a smaller earthquake using the same laws as for the triggering of a small earthquake by a previous larger one? Is the size of an earthquake predictable, based on its precursory activity, as in the "critical" earthquake model or can any small earthquake grow into a larger one, as predicted by ETAS model?
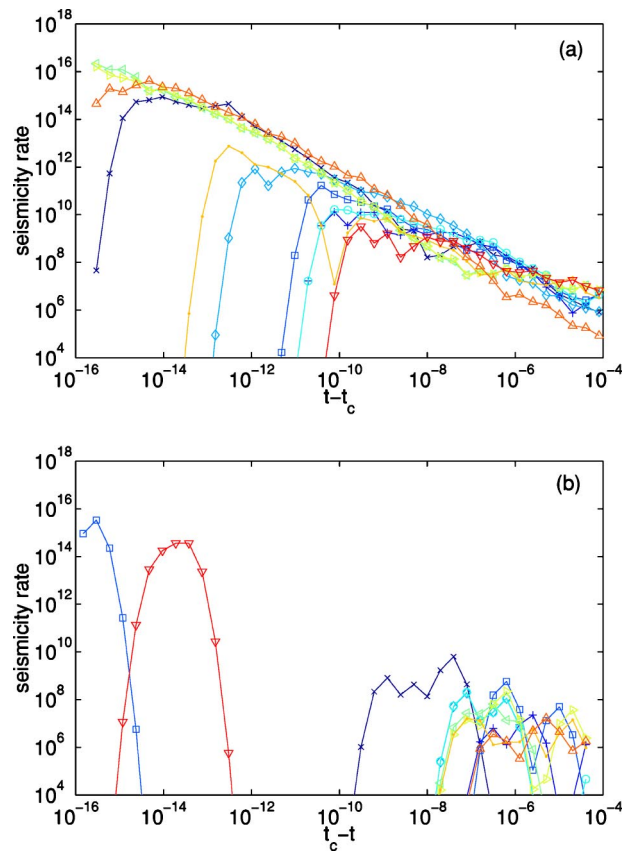

FIG. 1. (Color online) Ten individual sequences of aftershocks (a) and foreshocks (b), for mainshocks of size $s>2048$ with more than 1000 foreshocks or aftershocks, generated in a system of size $L=2048$, dissipation index $k=2$, and selected with definition $d=0$.

B. Omori's law (aftershocks) and inverse Omori's law (foreshocks)

Figure 1 shows the seismicity rate before ("foreshock sequence," bottom) and after ("aftershock sequence," top) 10 mainshocks of size $s>2048$. We have selected mainshocks with more than 1000 foreshocks or aftershocks, using definition $d=0$. We used a system of size $L=2048$ and a dissipation index $k=2$. Omori's law (6) is clear for each individual aftershock sequence while, for foreshocks, there is almost no increase of the seismic rate for individual sequences: the inverse Omori's law (7) is only observed when stacking many sequences, like in the ETAS model [16]. This suggests that the foreshock activity may be better described by a cascade ETAS-type model than by a critical earthquake model (but see below for other observations that may modulate this preliminary conclusion). The OFC model shares this property with real seismicity [23] and with the ETAS model [16].

We now describe the results obtained by averaging over a large number of sequences, which allow us to decrease the noise level and to look at smaller mainshocks. We have generated synthetic catalogs with the OFC model, using a lattice size $L=128, 256, 512, 1024, 2048$ and different values of the dissipation index $k=0.5, 1, 2, 4$. For each catalog, we have selected aftershocks and foreshocks following the different
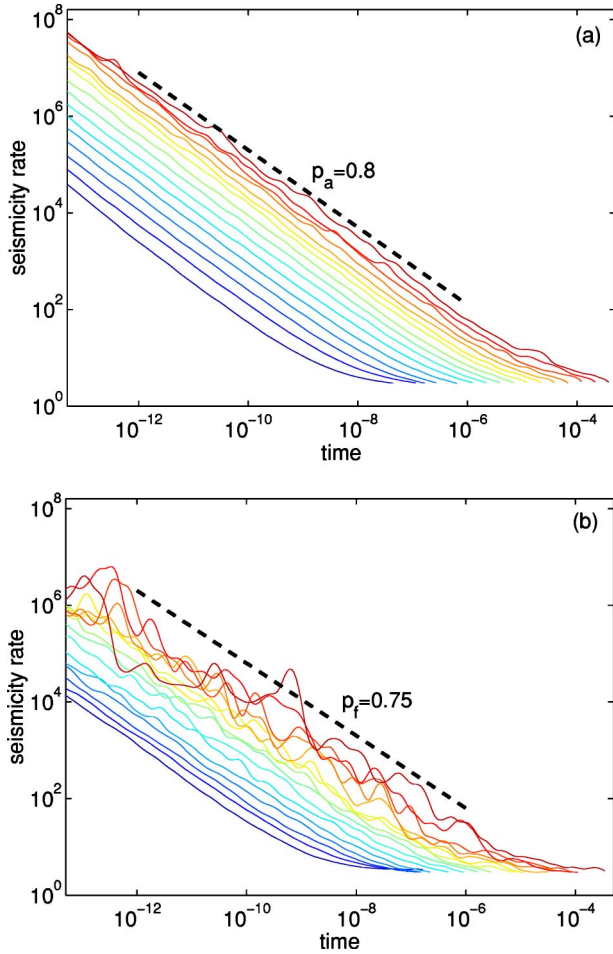
FIG. 2. (Color online) Omori's law [(a), aftershocks] and inverse Omori's law [(b), foreshocks] for synthetic catalogs generated with the OFC model with $L=2048$, dissipation index $k=2$, and definition $d=0$. The seismicity rate is normalized by the background rate and by the number of mainshocks in each class. The mainshock size increases from $s=2$ (bottom curve) to $s=2^{16}$ (top curve) with a factor of 2 between each curve.

definitions $d=0$, 1, 2 explained in Sec. V A. We have then stacked all sequences by superposing them translated in time so that the mainshock occurs at time $t=0$. We have first analyzed the change of the seismicity rate before and after a mainshock. For each range of mainshock size s between 2 and 2^{16}, increasing by a factor 2 between each class, we compute the average seismicity rate $N_f(t)$ and $N_a(t)$ as a function of the time before and after the mainshock. The results for $L=2048$, $k=2$, and $d=0$ are illustrated in Fig. 2. The rate of aftershocks obeys Omori's law (6) and the increase of the seismicity rate observed when averaging over many sequences follows the inverse Omori's law (7). We measure the Omori's exponents p_f and p_a by fitting the number $N_a(t)$ of aftershocks and the number $N_f(t)$ of foreshocks by a power law $\sim 1/|t|^{p_{a,f}}$ using a linear regression of $\ln(N)$ as a function of $\ln|t|$, in the time interval $|t| > 5 \times 10^{-14}$ and $|t| < t_{max}$, where the upper bound t_{max} is given by the condition that the seismicity rate is much larger than the background level.

For a mainshock of size $s=1024$ ($m \approx 5$), the rate of aftershocks goes back to the background level at $t_{OFC}=1.5 \times 10^{-5}$—i.e., about 9 days after the mainshock according to the correspondence (3). The actual aftershock duration should be larger, because our selection of aftershocks on the whole lattice of size 2048×2048 tends to increase the background and thus to reduce the time over which aftershocks can be observed above the background seismicity. We obtain a longer aftershock duration if we select as aftershocks earthquakes that occur up to one or two rupture lengths from the mainshock, as done for real seismicity.

Table I provides the values of the exponents p_a and p_f as a function of L, k, and d. We find similar Omori's exponents for foreshocks and aftershocks with $p_f \lesssim p_a < 1$. We observe the same time dependence of the seismicity rate (same exponents p_a and p_f) for all mainshock sizes, only the absolute value of the seismicity rate depends on the mainshock magnitude. The exponents p_a and p_f are found to increase with k from $p_a \approx 0.5$ for $k=0.5$ to $p_a \approx 0.9$ for $k=4$, but the duration of the aftershock and foreshock sequence does not change significantly with k. The number of foreshocks and aftershocks thus increases if the dissipation increases and is almost negligible in the nondissipative case. The Omori's exponents do not depend on the rules of selection d.

C. Dependence of the number of aftershocks and foreshocks with the mainshock size

Figure 3 represents the dependence of the number of aftershocks and foreshocks with the mainshock size, for different rules of selection $d=0$, 1, 2. We observe a power-law increase of the number of foreshocks K_f and aftershocks K_a defined in Eqs. (6) and (7) with the mainshock size s according to

$$K_a(s) \sim s^{\alpha_a}, \quad K_f(s) \sim s^{\alpha_f}, \tag{15}$$

for $s < 10^3$. The exponents α_a and α_f measured for $s < 1000$ increase with the dissipation index k (see Table I). The results are very similar for $d=1$ and $d=0$. The exponent α_a is slightly smaller for $d=1$ than for $d=0$, because for $d=0$ we impose aftershocks to be smaller than mainshocks. Small events are more likely to trigger an event larger than themselves than larger mainshocks and thus to be rejected from the analysis. Therefore the rule $d=0$ underestimates the number of earthquakes triggered by small mainshocks.

For $d=2$ and for small s, $K_a(s)$ and $K_f(s)$ are much larger than with $d=0$ and are almost independent of s for $s < 100$. This results from the fact that, for $d=2$, a significant fraction of "mainshocks" are triggered by a previous larger event, and thus the events classified as aftershocks may be in fact triggered by earthquakes that occurred before their "mainshock." The results obtained with $d=2$ recovers those obtained with $d=0$ and $d=1$ for large s. The correct value of the exponent α_a is thus the value obtained for $d=1$.

The number of foreshocks is generally smaller than the number of aftershocks and increases more slowly with s ($\alpha_f \lesssim \alpha_a$).

TABLE I. Aftershock and foreshock properties in the OFC model as a function of the system size L and of the dissipation index k, for different definitions of foreshocks and aftershocks d (see Sec. V A). b is the exponent of the cumulative distribution of avalanche sizes for the whole catalog (see Sec. V E). p_a and p_f are the Omori's exponents for aftershocks and foreshocks, respectively (see Sec. V B). α_a and α_f characterize the dependence of the aftershock and foreshock rates with the mainshock size s (see Sec. V C) in the range $s \leqslant 1024$. q_a and q_f describe the scaling of the aftershocks and foreshocks zone sizes with s (see Sec. V D), measured for $16 \leqslant s \leqslant 1024$. N_{1024} is the average number of aftershocks for a mainshock of size $1024 \leqslant s < 2048$, in a time window equal to 1% of the recurrence time of an event of size 1024.

k	L	b	d	p_a	p_f	α_a	α_f	q_a	q_f	N_{1024}
0.5	512	0.71	0	0.5	0.5	−0.2	−0.3			0.41
0.5	512		1	0.5	0.5	−0.2				0.44
0.5	512		2	0.5	0.5	−0.3	−0.5			0.50
0.5	1024	0.67	0	0.6	0.6	0.06	−0.29			0.58
0.5	1024		1	0.6	0.6	0.05	−0.21			0.66
0.5	1024		2	0.5	0.5	−0.42	−0.21			0.83
1	512	0.76	0	0.65	0.65	0.63	0.36			3.8
1	512		1	0.65	0.65	0.6	0.31			4.5
1	512		2	0.65	0.65	0.11	−0.1			7.0
1	1024	0.73	0	0.65	0.65	0.63	0.35	0.20	0.17	3.9
1	1024		1	0.65	0.65	0.58	0.34	0.19	0.13	5.2
1	1024		2	0.65	0.65	0.11	0.09	0.11	0.14	9.5
2	128	0.80	0	0.65	0.65	0.52	0.27	0.30	0.44	5.4
2	128		1	0.65	0.65	0.41	0.21	0.29	0.18	5.4
2	128		2	0.60	0.60	0.16	−0.1	0.27	0.01	5.6
2	256	0.81	0	0.75	0.75	0.77	0.57	0.35	0.29	20.0
2	256		1	0.70	0.70	0.67	0.52	0.31	0.26	24.0
2	256		2	0.70	0.70	0.21	0.01	0.21	0.03	31.0
2	512	0.80	0	0.75	0.75	0.82	0.64	0.37	0.37	29.0
2	512		1	0.75	0.75	0.75	0.61	0.31	0.32	43.0
2	512		2	0.75	0.75	0.16	0.01	0.13	0.06	88.0
2	1024	0.78	0	0.80	0.80	0.88	0.68	0.36	0.30	32.
2	1024		1	0.80	0.80	0.80	0.67	0.28	0.30	57.0
2	1024		2	0.75	0.75	0.14	0.03	0.08	0.07	138.0
2	2048	0.76	0	0.80	0.75	0.89	0.70	0.39	0.36	36.
2	2048		1	0.81	0.75	0.80	0.70	0.29	0.35	68.0
2	2048		2	0.80	0.75	0.11	0.00	0.07	0.09	215.0
4	512	0.95	0	0.85	0.80	0.90	0.71	0.34	0.40	187.0
4	512		1	0.85	0.80	0.77	0.66	0.23	0.39	257.0
4	512		2	0.80	0.80	0.22	0.07	0.10	0.19	410.0
4	1024	0.92	0	0.85	0.80	0.91	0.72	0.36	0.33	222.0
4	1024		1	0.80	0.80	0.78	0.66	0.26	0.30	379.0
4	1024		2	0.80	0.80	0.19	0.06	0.13	0.07	808.0

For large mainshock sizes $s > 1000$, we observe a saturation of K_a and K_f, and the number of foreshocks and aftershocks increases slower with s than predicted by Eqs. (15).

This saturation of the number of aftershocks for large mainshocks explains why the clustering in the OFC model is weaker than for real seismicity This saturation size does not depend either on k or on L. The effect of the system size L is only to change the shape of the functional form of $K_a(s)$ and $K_f(s)$ for large s: the saturation of $K_{a,f}(s)$ for $s > 1000$ is more obvious for smaller L.
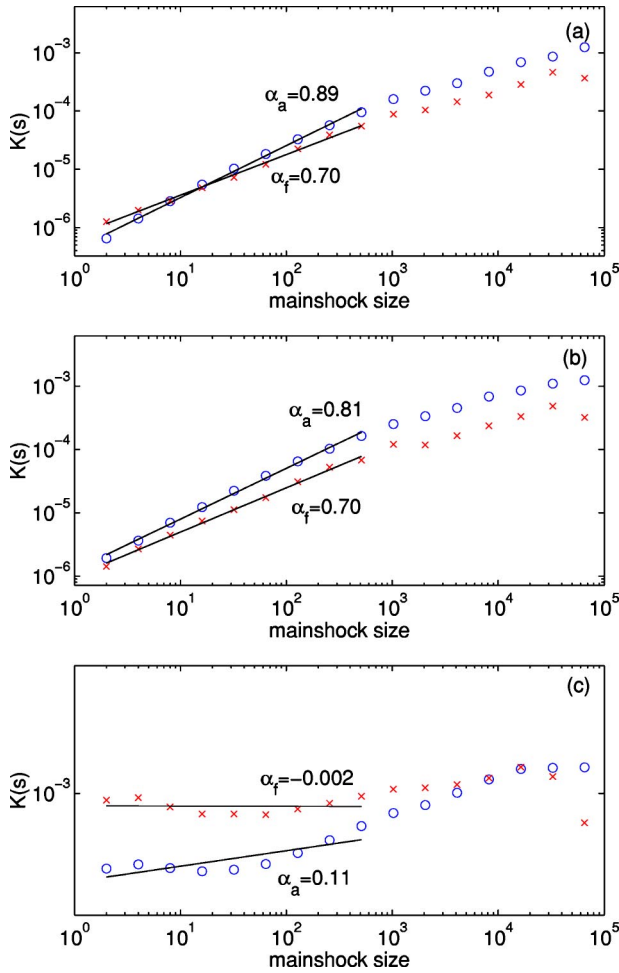
FIG. 3. (Color online) Number of aftershocks K_a (circles) and foreshocks K_f (crosses) as a function of the mainshock size s for synthetic catalogs generated with the OFC model with $L=2048$, dissipation index $k=2$, and definition $d=0$ (a), $d=1$ (b), and $d=2$ (c).

D. Spatial distribution of foreshocks and aftershocks

Figure 4 shows the stress field immediately before and after a large mainshock. Following the mainshock, many elements on the boundary of the avalanche and within the avalanche have been loaded by the rupture and are likely to generate aftershocks after the mainshock. There are a few large patches of elements within the avalanche that did not break during the mainshock, as illustrated in the lower panels of Fig. 4, but most aftershocks initiate on smaller clusters of a few unbroken elements shown as white spots in the central lower panel of Fig. 4. The density of such white spots observed in this square is typical of the rest of the stress field over the area spanned by the mainshock. In the language of seismicity, such white spots are "asperities" which carry a large stress after the mainshock and are nucleation point for future aftershocks. These white spots are also found on the avalanche boundaries.

The aftershock cluster size R_a, defined as the average distance between the mainshock and its aftershocks, is close to the mainshock size $\ell=\sqrt{s}$ at small times. At large times, the

proportion of uncorrelated events increases; therefore, R_a increases with time up to a value close to the system size L (see Fig. 5). We observe the same pattern for the spatial distribution of foreshocks. In the short-time regime where uncorrelated seismicity is negligible, we find a very weak, if any, diffusion of aftershocks, as measured by an increase $R_a \sim t^{H_a}$ of the aftershock zone size with the time after the mainshock. Similarly, we observe a very weak migration of foreshocks toward the mainshock, characterized by a decrease $R_f \sim (t_c-t)^{H_f}$ of the foreshock zone as the mainshock approaches. The exponents H_a and H_f are very close to 0, showing that the sizes of the foreshock and aftershock zones do not change significantly with time.

We observe on Fig. 6 a power-law increase of aftershock zone size and of the foreshock zone size with the mainshock size according to

$$R_a(s) \sim s^{q_a}, \quad R_f(s) \sim s^{q_f}, \tag{16}$$

in the range $10<s<10^4$. The exponents q_a and q_f are given in Table I as a function of k, L, and d. In contrast with real seismicity, the aftershock zone area is not proportional to the mainshock size $s^{0.5}$, but it increases slower with s ($q_a \approx 0.3<0.5$ for $d=0$ or 1). This is probably due to the effect of secondary aftershocks, which increase the effective size of the aftershock zone for small mainshocks. Secondary aftershocks are more important for $d=1$ than for $d=0$, which explains why q_a is smaller for $d=1$ than for $d=0$. The average value of the foreshock zone ("zone of mainshock preparation") is smaller than the aftershock zone, except for definition $d=2$.

An increase of R_f with s according to Eqs. (16) has been reported by Refs. [25,26] for individual sequences, with an exponent $q_f=0.44$ [26], but was not observed by Ref. [23] when using stacked sequences and when allowing foreshocks to be larger that the mainshock ($d=2$). This increase of R_f with s is not observed by the ETAS model, because the magnitude of each earthquake is drawn at random, independently of previous seismicity, and thus all properties of foreshocks must be independent of the mainshock size.

For $d=2$, the average zone sizes R_a and of R_f are much larger than for $d=0$, because we include foreshocks and aftershocks larger than the mainshock. For $s<1000$, the values of R_a and R_f are almost constant of the order of $R_{a,f} \approx 100$. This may reflect the fact that, for $d=2$ and for small mainshocks, most aftershocks are not triggered by the mainshock but by a previous larger event.

E. Distribution of avalanche sizes

For the whole catalogs, the distribution of event sizes is a power law characterized by an exponent b, with an exponential roll-off for large sizes $s>10^{-3}L^2$. Table I shows that the exponent b increases as the dissipation index increases, from $b \approx 0.7$ for $k=0.5$ to the realistic value $b \approx 0.95$ for $k=4$, in agreement with previous works [10,51].

Figure 7 tests the stationarity of the magnitude distribution for foreshocks and aftershocks. The magnitude distributions for foreshocks and aftershocks have been fitted with expression (11) and these fits are shown as the solid lines.
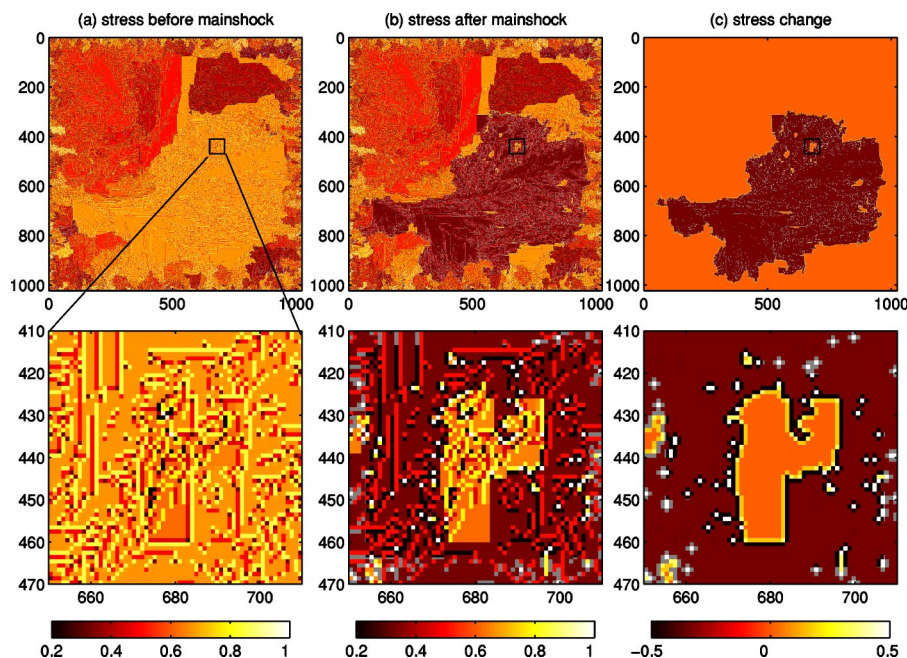
FIG. 4. (Color online) Stress field immediately before (a) and after (b) a mainshock. The stress change due to the mainshock in shown in (c). The elements that broke during the avalanche are shown in dark in (c) (stress decrease) and were mostly close to the rupture threshold before the mainshock [light gray in (a)]. The upper panels show the whole grid of size $L=1024$ and the lower plots represent a subset of the grid delineated by the square in the upper plot.

The deviation of the magnitude distribution from the average GR law for foreshocks and aftershocks are well represented by Eq. (11) with b' in the range 0.3–0.5 and with $Q(t)$ increasing as a power law according to Eq. (13) with $\nu \approx 0.1$ for foreshocks and for aftershocks.

For aftershocks, the time dependence of $Q(t)$ describes a decrease of the deviation from the GR law for latter aftershocks. While these fits are good, there is an important caveat: the prediction $b'=b-\alpha_a$ of the ETAS model is not verified here, as the OFC model gives $b' \approx 0.4$ and $\alpha_a \approx b$.

The modification of the magnitude distribution for aftershocks in the OFC model is much weaker than for foreshocks, but is significant. This implies that the magnitude distribution in the OFC model is not stationary because the magnitude of triggered earthquakes is correlated with the mainshock magnitude, in contradiction with a crucial hypothesis of the ETAS model and with real catalogs. Figure 8 shows that, for $d=1$ (no constraint on aftershock magnitudes), the change of the magnitude distribution is almost independent of the mainshock magnitude (like in the ETAS model). However, there is a larger proportion of medium-size events for smaller mainshocks than for larger ones. This means that smaller mainshocks have a tendency to trigger smaller aftershocks than larger mainshocks.

This result is in contradiction with the ETAS model, which does not reproduce a dependence of the aftershock magnitude as a function of the size of the triggering earthquake or as a function of the time since the mainshock. Observations of real seismicity [17] do not show any dependence between the aftershock magnitude and the mainshock magnitude, but the catalogs available are much smaller than for our OFC simulations.

VI. MECHANISMS FOR FORESHOCKS AND AFTERSHOCKS IN THE OFC MODEL

Is the increase of the number of aftershocks and foreshocks with the mainshock magnitude real or is it just the result of a selection bias introduced by the standard definition $d=0$, which requires that mainshocks are the largest events in the cluster? Indeed, in the OFC catalogs, the clear power-law increase of the number of aftershocks and foreshocks with the size s of the mainshock, found when we define the mainshock as the largest event ($d=0$), almost disappears when aftershocks or foreshocks are not constrained to be smaller than the mainshock ($d=2$), as shown in Fig. 3. The question of the impact of the definition is thus essential.

For foreshocks, we consider two possible interpretations, the ETAS model described in Sec. IV A and the critical earthquake model (CEM) summarized in Sec. IV B. The fact that, using $d=0$, both the number of foreshocks and the average foreshock cluster size increase with the mainshock size s seems to favor the critical model, but Ref. [16] has shown that the constraint that foreshocks must be smaller than the mainshock ($d=0$) leads to an artificial increase of the number of foreshocks and of the foreshock cluster size with s (see Fig. 5 of [16]). However, this spurious increase of the number of foreshocks with the mainshock magnitude should be observed only for small s and should not exist in the case $d=2$ (without constraints on foreshock and mainshock magnitudes). The fact that a weak increase of the number of foreshocks with s is observed even for very large s and for all definitions $d=0$, 1, 2 suggests that the effect is genuine. Such a dependence of foreshock properties on the mainshock size cannot be reproduced with the ETAS model, but sug-
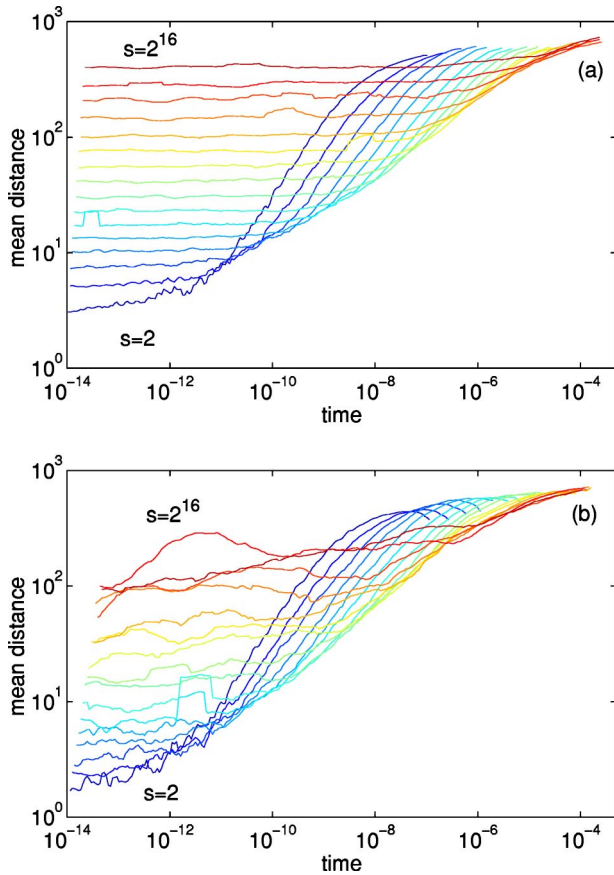
FIG. 5. (Color online) Average distance between mainshocks and aftershocks (a) and mainshocks and foreshocks (b) as a function of the time after (a) or before (b) the mainshock, for synthetic catalogs generated with the OFC model with $L=2048$, dissipation index $k=2$, and definition $d=0$. Each curve corresponds to a different mainshock size increasing from $s=2$ (bottom curve) to $s=2^{16}$ (top curve) with a factor of 2 between each curve.

FIG. 6. (Color online) Average distances R_a (circles) and R_f (crosses) as a function of the mainshock size s, for $k=2$, $L=2048$, and for definitions $d=0$ (a), $d=1$ (b), and $d=2$ (c). The lines are fits of $R_{a,f}(s)$ by a power law s^q according to Eq. (16).

gests that the critical model provides a more relevant description of these observations.

The case $d=2$ destroys the dependence of the aftershock number with s for small s, which is a real physical property of aftershocks because it is also observed for $d=1$. The same effect may also be at work for foreshocks and explain why, if the properties of foreshocks are physically dependent on the mainshock magnitude, this dependence is not observed when using $d=2$. Definition $d=2$ may be mixing "critical foreshocks"—i.e., events that belong to the preparation phase of the future mainshock—with "triggering-triggered" pairs (which are the usual "foreshock-mainshock" pairs in the ETAS model). Thus, the absence of conditioning ($d=2$) seems to destroy the dependence of both the foreshock and aftershock properties with the mainshock magnitudes—i.e., $\alpha_{a,f} \approx 0$ and $q_{a,f} \approx 0$ both for foreshocks and aftershocks. But for aftershocks, we know it to be true that the dependence of the number (α_a) and the cluster size (q_a) are real and physical because they are observed in the case $d=1$ which do not constrain aftershocks to be smaller than the mainshocks.

For aftershocks selected according to $d=2$ and for small mainshock sizes s, the scenario, according to which most
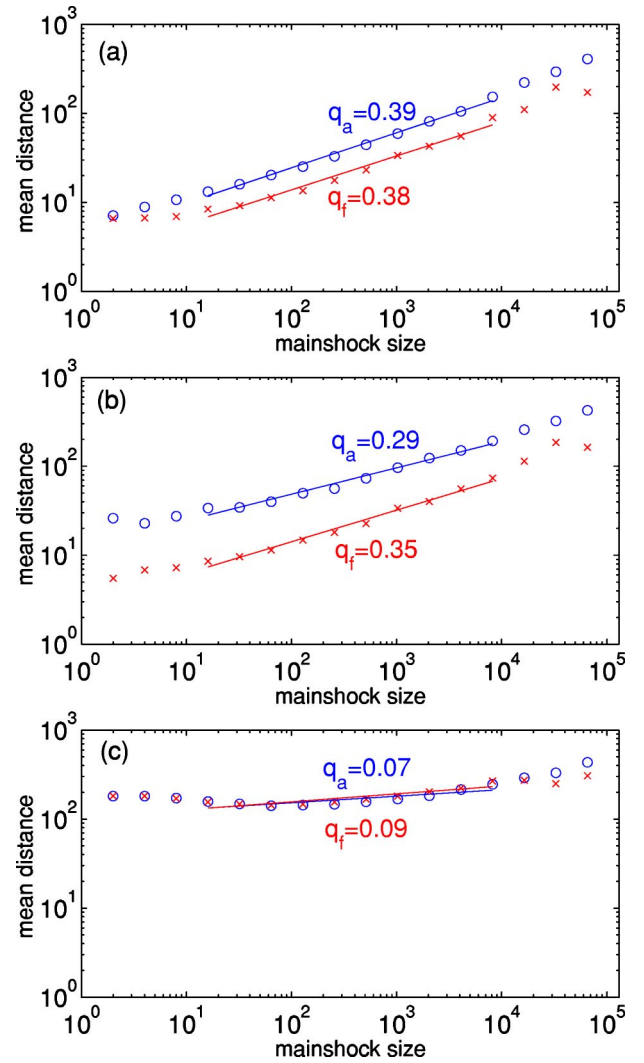
aftershocks are not triggered by the mainshock *per se* but by a previous larger event, seems to explain both the fact that (i) the number of aftershocks is almost constant with s for $s < 100$ and (ii) the size of the aftershock cluster is almost constant with s for small s. It is, however, surprising, if this interpretation is correct, that we observe a pure Omori's law for aftershocks and foreshocks in the case $d=2$, without any change in the Omori's exponent with s and without any roll-off at small times.

In order to better understand the mechanism responsible for aftershocks in the OFC model, we have imposed several types of perturbations to the normal course of an OFC simulation to obtain the response of the system. First, we have simulated random isolated disturbances consisting in choosing randomly and independently 1024 sites and adding to them random amounts of stress drawn in the interval [0, 0.01] or [0, 0.1]. Repeating such disturbance 100 000 times, we find no observable seismicity triggered by this perturbation. This shows that the aftershocks require a coherent spa-
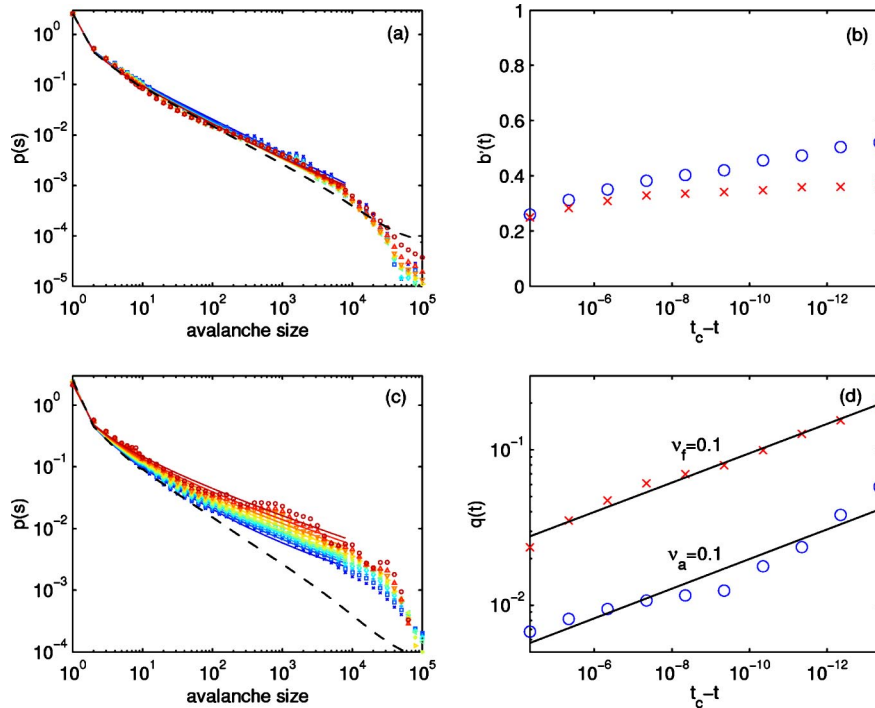
FIG. 7. (Color online) Aftershock (a) and foreshock (c) size distributions as a function of the time before or after the mainshock, for $k=2$ and $L=1024$, and for a mainshock size in the range $s=2048-4096$. Aftershocks were selected with $d=1$ and foreshocks with $d=2$ (without constrains on the magnitude of foreshocks and aftershocks). The avalanche size distributions are constructed with a logarithmic binning (linear bin in magnitudes), whose slope gives the GR b value. The dashed line in (a) in (c) shows the size distribution for the whole catalog for reference. The different curves correspond to different time windows closer and closer to the mainshock, from $|t_c-t|=5\times10^{-5}$ (crosses) to $|t_c-t|=5\times10^{-14}$ (circles). The solid lines in (a) and (c) are the fit of the foreshock and aftershock size distribution $P(s)$ for $s<10^4$ as defined in expression (11). The corresponding values of $b'(t)$, Eq. (12), and $Q(t)$, Eq. (13), are shown in (b) and (d) for foreshocks (crosses) and aftershocks (circles), as a function of time before or after the mainshock.

tial organization over a broad area. In contrast, pasting (or grafting) the stress map as shown in Fig. 4 of those sites that participated in a given large mainshock in a given simulation and their nearest neighbors onto another independent simulation gives a perfect Omori's law following this graft in this second simulation as if the foreign stress map of the first simulation was part of the second simulation. The resulting aftershock sequences are similar to natural sequences. This demonstrates that the presence of asperities close to the failure threshold inside the boundary of the avalanche can produce realistic aftershock sequences with an Omori's law temporal decay. To investigate further if it is the spatial connectivity of the perturbation which is important to get aftershocks, we have also raised simultaneously the stress by various amounts within squares of size 64×64. Performing this perturbation 40 000 times at random instants, we observe that this sometimes results in quite large earthquakes immediately following the perturbation, but there is no significant activity afterwards and nothing that looks like an Omori's law of aftershocks. Thus, it seems impossible to generate aftershocks by introducing a random or deterministic spatially extended perturbation. This suggests that aftershocks require not only the occurrence of mainshocks to redistribute stress but also a spatial organization of the stress field prior to the mainshock so that many "asperities" (as illustrated in Fig. 4) can be created by the interplay of the

stress organization before the mainshock and the stress redistribution by the mainshock.

VII. CONCLUSION

The results obtained in this paper can be viewed from two different perspectives. On the one hand, we are adding to the phenomenology of one of the most studied model of self-organized criticality. Extending Hergarten and Neugebauer's announcement [3], we have shown evidence that the self-organized critical state of the OFC model is much richer than previously thought, with important correlation patterns in space and time between avalanches. We have obtained quantitative scaling laws describing the spatiotemporal clustering of events in the OFC model. On the other hand, we have shown that what is probably the simplest possible mechanism for the generation of earthquakes (slow tectonic loading and sudden stress relaxation with local stress redistribution) is sufficient to recover essentially all known properties documented in seismic catalogs, at a qualitative level. Specifically, we have found that foreshocks and aftershocks follow Omori's power laws, as in real seismicity but with smaller exponents.

We have found the same scaling of the number of aftershocks with the mainshock size as in real seismicity. In contrast with real seismicity, we also found a power-law increase
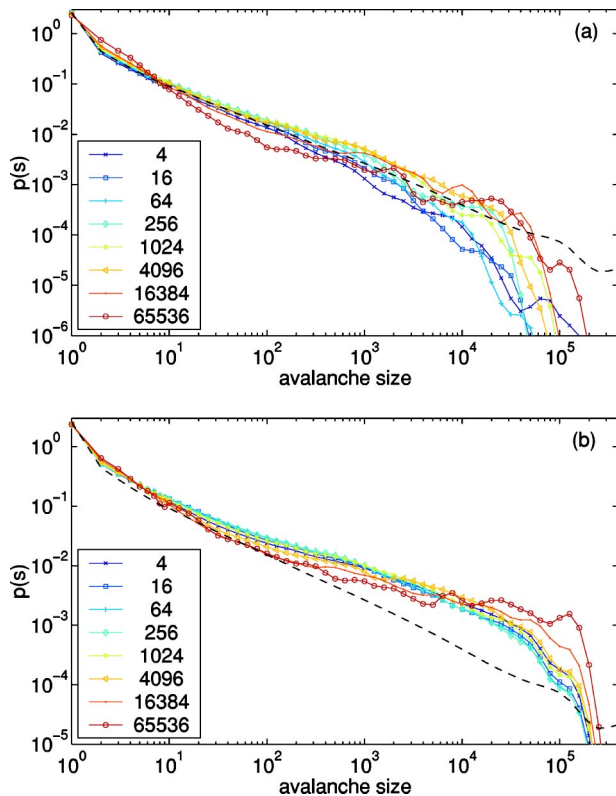
FIG. 8. (Color online) Aftershock (a) and foreshock (b) size distributions as a function of the mainshock size, for $k=2$ and $L=1024$. Aftershocks ($d=1$) and foreshocks ($d=2$) are selected in a time window $5 \times 10^{-11} < |t_c - t| < 5 \times 10^{-10}$. Each curve corresponds to a different mainshock size between $s=4$ and $s=2^{16}$ (see legend). The dashed line shows the (unconditional) distribution of the whole catalog.

of the number of foreshocks with the mainshock size. The nucleation of aftershocks at "asperities" located on the mainshock rupture plane or on the boundary of the avalanche is also in agreement with observations. These findings are interesting because they add on the list of possible mechanisms for foreshocks and aftershocks that have been discussed previously in the literature.

We also found that the predictability increases with the mainshock magnitude in the OFC model, because the number of foreshocks seems to increase with the magnitude of the mainshock, a feature that is not observed in real seismicity [23]. See the debate in Nature at http://helix.nature.com/debates/earthquake/ and [52,53] for related discussions on the predictability of real earthquakes and the use of models from statistical physics.

We have systematically compared the statistical properties of the avalanches generated by the dynamics of the OFC model with those predicted by the ETAS model on the one hand and by the critical earthquake model on the other hand. These two models constitute end-member models of seismicity. While most of the OFC dynamics can be qualitatively captured by the ETAS model, this property that the number of foreshocks seems to increase with the magnitude of the mainshock is better explained by the critical earthquake model. This suggests a picture in which future avalanches are triggered by past avalanches through "asperities" located either within the plane of past avalanches or at their boundaries. In addition, we find that this triggering mechanism presents a degree of cooperativity, as the number of foreshocks increases with the mainshock size. In other words, this suggests that asperities interact via avalanches, and when their number and size increase in a given location, they can produce larger avalanches.

[1] B. Gutenberg and C. F. Richter, Bull. Seismol. Soc. Am. **34**, 185 (1944).

[2] F. Omori, J. Coll. Sci., Imp. Univ. Tokyo **7**, 111 (1894).

[3] S. Hergarten and H. J. Neugebauer, Phys. Rev. Lett. **88**, 238501 (2002).

[4] Y. Ogata, J. Am. Stat. Assoc. **83**, 9 (1988).

[5] Z. Olami, H. J. S. Feder, and K. Christensen, Phys. Rev. Lett. **68**, 1244 (1992).

[6] R. Burridge and L. Knopoff, Bull. Seismol. Soc. Am. **57**, 341 (1967).

[7] P. Bak, *How Nature Works: the Science of Self-organized Criticality* (Copernicus, New York, 1996).

[8] H. J. Jensen, *Self-Organized Criticality* (Cambridge University Press, Cambridge, England, 1998).

[9] D. Sornette, *Critical Phenomena in Natural Sciences*, 2nd ed. Springer Series in Synergetics (Springer, Heidelberg, 2004).

[10] P. Grassberger, Phys. Rev. E **49**, 2436 (1994).

[11] Y. Huang, H. Saleur, C. G. Sammis, and D. Sornette, Europhys. Lett. **41**, 43 (1998).

[12] Y. Y. Kagan and L. Knopoff, Geophys. J. R. Astron. Soc. **55**, 67 (1978).

[13] T. Utsu, Y. Ogata, and S. Matsu'ura, J. Phys. Earth **43**, 1 (1995).

[14] B. C. Papazachos, Bull. Seismol. Soc. Am. **63**, 1973 (1973).

[15] L. M. Jones and P. Molnar, J. Geophys. Res. **84**, 3596 (1979).

[16] A. Helmstetter, D. Sornette, and J.-R. Grasso, J. Geophys. Res., [Solid Earth] **B108**, 2046 (2003).

[17] A. Helmstetter, Phys. Rev. Lett. **91**, 058501 (2003).

[18] F. Tajima and H. Kanamori, Phys. Earth Planet. Inter. **40**, 77 (1985).

[19] D. Marsan, C. J. Bean, S. Steacy, and J. McCloskey, J. Geophys. Res., [Solid Earth] **B105**, 28 081 (2000).

[20] B. E. Shaw, Geophys. Res. Lett. **20**, 907 (1993).

[21] A. Helmstetter, G. Ouillon, and D. Sornette, J. Geophys. Res., [Solid Earth] **B108**, 2483 (2003).

[22] D. von Seggern, S. S. Alexander, and C.-B. Baag, J. Geophys. Res. **B86**, 9325 (1981).

[23] A. Helmstetter and D. Sornette, J. Geophys. Res., [Solid Earth] **B108**, 2457 (2003).

[24] Y. Y. Kagan, Bull. Seismol. Soc. Am. **92**, 641 (2002).

[25] V. I. Keilis-Borok and L. N. Malinovskaya, J. Geophys. Res. **69**, 3019 (1964).

[26] D. D. Bowman, G. Ouillon, C. G. Sammis, A. Sornette, and D. Sornette, J. Geophys. Res. **B103**, 24359 (1998).

[27] Y. Y. Kagan and L. Knopoff, Phys. Earth Planet. Inter. **12**, 291 (1976).

[28] Y. Y. Kagan and L. Knopoff, J. Geophys. Res., [Solid Earth] **B86**, 2853 (1981); Science **236**, 1563 (1987).

[29] P. Alstrom, Phys. Rev. A **38**, 4905 (1988).

[30] Y. Y. Kagan and D. D. Jackson, J. Geophys. Res., [Solid Earth] **B103**, 24453 (1998).

[31] A. Helmstetter and D. Sornette, J. Geophys. Res., [Solid Earth] **B107**, 2237 (2002).

[32] D. Vere-Jones, Math. Geol. **9**, 455 (1977).

[33] C. J. Allegre, J. L. Le Mouel, and A. Provost, Nature (London) **297**, 47 (1982).

[34] P. J. Reynolds, W. Klein, and H. E. Stanley, J. Phys. C **10**, L167 (1977).

[35] B. Voight, Nature (London) **332**, 125 (1988).

[36] B. Voight, Science **243**, 200 (1989).

[37] C. G. Bufe and D. J. Varnes, J. Geophys. Res., [Solid Earth] **B98**, 9871 (1993).

[38] D. Sornette and C. G. Sammis, J. Phys. I **5**, 607 (1995).

[39] A. Sornette and D. Sornette, Tectonophysics **179**, 327 (1990).

[40] S. C. Jaumé and L. R. Sykes, Pure Appl. Geophys. **155**, 279 (1999).

[41] G. Ouillon and D. Sornette, Geophys. J. Int. **143**, 454 (2000).

[42] P. Mora and D. Place, Pure Appl. Geophys. **159**, 2413 (2002).

[43] G. Zöller and S. Hainzl, Nat. Hazards Earth Syst. Sci. **1**, 93 (2001).

[44] G. Zöller, S. Hainzl, and J. Kurths, J. Geophys. Res., [Solid Earth] **B106**, 2167 (2001).

[45] G. Zöller and S. Hainzl, Geophys. Res. Lett. **29**, 10.1029/2002GL014856 (2002).

[46] S. G. Sammis and D. Sornette, Proc. Natl. Acad. Sci. U.S.A. **99**, (Suppl. 1), 2501 (2002).

[47] G. M. Molchan and O. E. Dmitrieva, Geophys. J. Int. **109**, 501 (1992).

[48] S. E. Hough and L. M. Jones, EOS Trans. Am. Geophys. Union **78**, 505 (1997).

[49] L. M. Jones, R. Console, F. Di Luccio, and M. Murru, EOS Trans. Am. Geophys. Union **76**, Suppl., F388 (1995).

[50] K. R. Felzer, T. W. Becker, R. E. Abercrombie, G. Ekström, and J. R. Rice, J. Geophys. Res., [Solid Earth] **B107**, 2190 (2002).

[51] S. Lise and M. Paczuski, Phys. Rev. E **63**, 036111 (2001).

[52] S. L. Pepke and J. M. Carlson, Phys. Rev. E **50**, 236 (1994).

[53] R. J. Geller, D. D. Jackson, Y. Y. Kagan, and F. Mulargia, Science **275**, 1616 (1997).